THE ASTROPHYSICAL JOURNAL, 494:247–255, 1998 February 10

CHEMODYNAMICAL MODEL OF THE GALAXY: ABUNDANCE GRADIENTS PREDICTED FOR H II REGIONS AND PLANETARY NEBULAE

CHRISTINE ALLEN, LETICIA CARIGI, AND MANUEL PEIMBERT
Instituto de Astronomía, UNAM Apdo. Postal 70-264, DF 04510, Mexico
Received 1997 June 16; accepted 1997 September 19

ABSTRACT

We present a chemodynamical evolution model of the Galaxy to determine chemical abundance gradients of different stellar populations. From this model we have determined the abundance gradients expected for H II regions, as well as for planetary nebulae of different ages and different kinematical properties. We have compared the model predicted gradients with those derived from planetary nebulae (PNs) of types I, II, and III. From this comparison we conclude that only about half of the stars evolving toward the white dwarf stage produce PNs and that the less massive stars are less likely to produce PNs. Other arguments supporting the previous conclusions are presented.

Subject headings: Galaxy: abundances — Galaxy: evolution — Galaxy: kinematics and dynamics — planetary nebulae: general — stars: evolution

1. INTRODUCTION

Abundance gradients of H II regions provide strong constraints for models of Galactic chemical evolution (e.g., Carigi 1996 and references therein). Similarly, planetary nebulae (PNs) abundance gradients can be used to test models of Galactic chemical evolution. PNs are produced by intermediate-mass stars (IMSs) in their transition from red giants to white dwarfs. IMSs have initial masses in the $0.83 < m(M_\odot) < 8.41$ range (Peimbert 1990a). The wide range of initial masses implies that the progenitors of PNs have also a wide range of ages. The abundances of elements like O, Ne, S, and Ar observed in PNs correspond to the abundances of the interstellar medium at the time their progenitor stars were formed, since IMSs do not form or destroy these elements during their evolution.

To compare our model with observations, we will follow the classification of PNs by Peimbert (1978). Type I PNs are those that are He and N rich and comprise the most massive IMSs, those with initial masses in the $2.02 < m(M_\odot) < 8.41$ range (see Torres-Peimbert & Peimbert 1997, and references therein, for a recent review on type I PNs). Type II PNs are those with masses smaller than about 2 $M_\odot$ and low velocities, and type III PNs are those with masses smaller than about 2 $M_\odot$ and high velocities that do not belong to the halo. We will compare our computed radial gradients with those derived by Maciel & Köppen (1994) for PNs of types I, II, and III. Recent reviews on gradients derived from PNs have been presented by Maciel (1996, 1997).

Some of the aims of this paper are (*a*) to study the variation of the radial abundance gradients with time; (*b*) to try to define the mass and velocity boundaries between different types of PNs more precisely; (*c*) to estimate if all IMSs become PNs; (*d*) to test the assumptions on which our chemodynamical model is based; (*e*) to study the effect on the Galactocentric distances of individual stars of encounters with spiral arms, giant molecular clouds, and so on, during their lifetimes; and (*f*) to predict vertical abundance gradients for different Galactocentric distances.

2. CHEMICAL EVOLUTION

This section presents the main features of our chemical evolution model and some model results. In this investigation we centered our attention on the values of the H and O abundances in the gas and on the number of present-day planetary nebulae.

2.1. *Assumptions*

We have computed an infall model of primordial gas for the Galactic disk formation, for which the central regions of the disk form faster than the outskirts. The Galactic disk, with an age of $t_g = 13$ Gyr (Rana 1991), is represented by concentric rings, each 1 kpc wide. Radial flows and outflows are not considered. This model is very similar to the "best model" shown in Carigi (1996), except that the stellar yields are different in the $11 \leq m(M_\odot) \leq 85$ range (see below).

The star formation rate is proportional to a power of the surface mass gas density σ_g and the total surface mass density σ_T:

$$\Psi(r, t) = 0.0156\sigma_g(r, t)^{1.4}\sigma_T(r, t)^{0.4} . \quad (1)$$

We have adopted an infall rate such that the G-dwarf distribution in the solar neighborhood (Rocha-Pinto & Maciel 1996), and the stellar profile of the Galactic disk (Gilmore 1989), are reproduced at the right age.

According to Lacey & Fall (1985), the infall rate can be expressed as

$$\dot{\sigma}_f = \frac{\sigma_T(r_\odot, t_g)}{(1 - e^{-t_g/\tau(r)})\tau(r)}\, e^{-(r-r_\odot)/3\ \mathrm{kpc}} e^{-t/\tau(r)} , \quad (2)$$

where $\tau(r) = 24/7(r/r_\odot - 1/8)$ Gyr, $r_\odot = 8$ kpc is the distance of the Sun to the Galactic center, and $\sigma_T(r_\odot, t_g) = 45$ $M_\odot$ pc^{-2} (Kuijken & Gilmore 1991). For $\dot{\sigma}_f$ we have assumed that the radial profile of the total mass has the same exponential scale length as the stellar mass distribution, which is a good approximation for $r < 12$ kpc (Prantzos & Aubert 1995).

The adopted initial mass function (Kroupa, Tout, & Gilmore 1993) is constant in time and space, with a mass range extending from 0.01 to 85 $M_\odot$.

All stellar properties are dependent on the initial metallicity of the progenitor gas clouds. The model does not use the instantaneous recycling approximation. We have assumed that progenitor stars of Type II supernovae eject their whole envelope just after the H-burning phase, while the stars that eventually turn into PNs do it at the end of

the He-burning phase. The main-sequence lifetimes are taken from Schaller et al. (1992) and, for the horizontal and early asymptotic giant branches, from Charbonnel et al. (1996).

Stellar yields are taken from Renzini & Voli (1981) for $0.8 < m(M_\odot) \leq 8$, from Woosley & Weaver (1995) for $11 \leq m(M_\odot) \leq 40$, and from Woosley, Langer, & Weaver (1993) for $40 < m(M_\odot) \leq 85$, to take into account the most recent model results.

2.2. *Results*

In this subsection we discuss the main results obtained from the model explained above. Table 1 summarizes the main model predictions for the solar neighborhood, which have been used in combination with dynamical results and other assumptions (see below) to obtain the PNs' gradient. In the first column we present the mean age of the planetary nebula progenitors, (PNPs). Columns (4), (6), and (8) present the number of progenitors of the present-day stars in the PNs phase, normalized to the total number of these progenitors over the whole disk, $N/N_{\rm tot}$ within the mass range shown in the second column. Columns (3), (5), and (7) give the O/H abundance at the radii where these progenitors were supposedly formed.

Figure 1 presents the results for the present-day O/H radial gradient and for σ_g. The efficiency constant in equation (1) was chosen for the model to reproduce the surface gas mass density and the O/H derived from H II regions in the solar neighborhood.

It is clear from Figure 1*a* that the predicted present-day O/H gradient (-0.115 dex kpc^{-1}) is steeper than suggested by observations of Vílchez & Esteban (1996) (-0.036 dex kpc^{-1}) of H II regions with $r > 12$ kpc. The use of the yields of Woosley & Weaver (1995) has eliminated the convex behavior of the O/H gradient from the "best model" in Carigi (1996).

Figure 1*b* shows that the predicted $\sigma_g(r, t_g)$, within $3 < r(\text{kpc}) < 5$ is lower (by ~ 0.2 dex) than the observational limits. Initially, our model consumes the gas much faster in the inner regions relative to the outer ones, since star formation is more efficient in the inner regions. Later on, the strong decline of the infall rate keeps $\sigma_g(r, t_g)$ below the observed values.

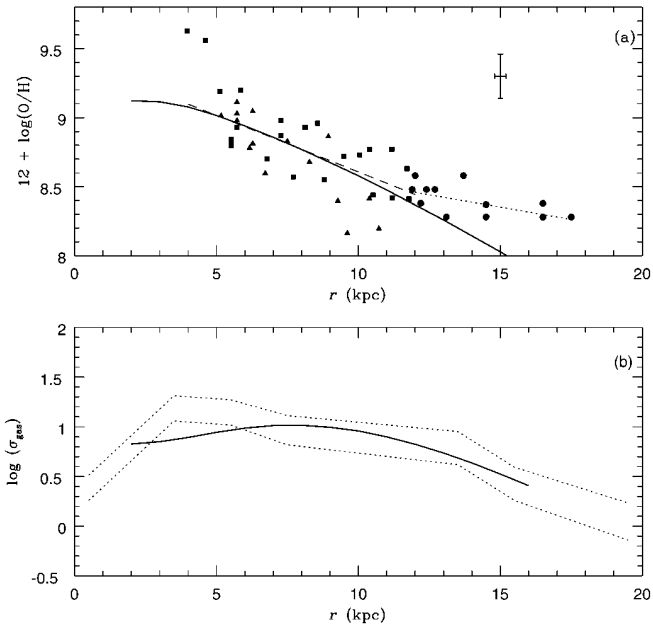

FIG. 1.—The present-day radial distributions of (*a*) O/H and (*b*) gas surface mass density (*solid lines*). O/H observations in (*a*) are marked as follows: *squares*, Shaver et al. (1983); *triangles*, Peimbert (1979); *circles*, Vílchez & Esteban (1996). Dashed and dotted lines show the gradients suggested by Shaver et al. (1983) and by Vílchez & Esteban (1996) (case B), respectively. Assuming that 20% of the Oxygen is locked in dust, 0.08 dex have been added to the observed O/H from the sources. A cross shows typical errors of the data sample. The observed gas profile in (*b*) is taken from Dame (1993) normalized to the σ_g ($r_\odot$) of Rana & Basu (1992) and Kuijken & Gilmore (1989). The area enclosed by dotted lines in (*b*) indicates the data collected by Prantzos & Aubert (1995).

Figure 2 shows the O/H abundance gradient for the gas and the radial distribution of PNPs born from this gas at three different times (2.5, 8.5, and 12.3 Gyr), or equivalent ages (10.5, 4.5, and 0.7 Gyr). Both distributions flatten with time, but they do so faster toward the central parts and more slowly at the outer regions. This time evolution of the gradient is again a reflection of the particular modeling of the formation history of the Galactic disk and of the

TABLE 1

CHEMICAL EVOLUTION FOR THE SOLAR NEIGHBORHOOD[a]

AGE (Gyr)	$m(M_\odot)$	$r = 7$ kpc		$r = 8$ kpc		$r = 9$ kpc	
		O/H	$N/N_{\rm tot}$	O/H	$N/N_{\rm tot}$	O/H	$N/N_{\rm tot}$
12.8.....	0.833–0.840	6.26	7.25×10^{-11}	6.09	5.92×10^{-11}	5.93	4.78×10^{-11}
12.1.....	0.840–0.850	7.10	8.66×10^{-4}	6.94	4.40×10^{-4}	6.78	2.26×10^{-4}
11.5.....	0.850–0.869	7.62	4.13×10^{-3}	7.47	2.25×10^{-3}	7.31	1.21×10^{-3}
10.5.....	0.869–0.890	7.97	6.73×10^{-3}	7.82	3.99×10^{-3}	7.68	2.30×10^{-3}
9.5.....	0.890–0.914	8.19	7.98×10^{-3}	8.05	5.17×10^{-3}	7.91	3.19×10^{-3}
8.5.....	0.914–0.942	8.34	8.43×10^{-3}	8.21	5.92×10^{-3}	8.08	3.90×10^{-3}
7.5.....	0.942–0.975	8.45	8.41×10^{-3}	8.33	6.34×10^{-3}	8.21	4.43×10^{-3}
6.5.....	0.975–1.018	8.54	8.58×10^{-3}	8.43	6.87×10^{-3}	8.31	5.07×10^{-3}
5.5.....	1.018–1.080	8.61	8.97×10^{-3}	8.50	7.58×10^{-3}	8.39	5.87×10^{-3}
4.5.....	1.080–1.167	8.67	9.11×10^{-3}	8.57	8.05×10^{-3}	8.46	6.50×10^{-3}
3.5.....	1.167–1.292	8.72	8.57×10^{-3}	8.62	7.86×10^{-3}	8.52	6.59×10^{-3}
2.5.....	1.292–1.481	8.77	7.79×10^{-3}	8.67	7.39×10^{-3}	8.57	6.41×10^{-3}
1.5.....	1.481–2.023	8.81	9.73×10^{-3}	8.71	9.50×10^{-3}	8.62	8.49×10^{-3}
0.7.....	2.023–2.731	8.83	5.45×10^{-3}	8.74	5.43×10^{-3}	8.65	4.95×10^{-3}
0.3.....	2.731–4.111	8.85	4.26×10^{-3}	8.76	4.28×10^{-3}	8.66	3.95×10^{-3}
0.1.....	4.111–8.406	8.85	2.78×10^{-3}	8.77	2.81×10^{-3}	8.67	2.60×10^{-3}

[a] O/H = 12 + log (O/H).

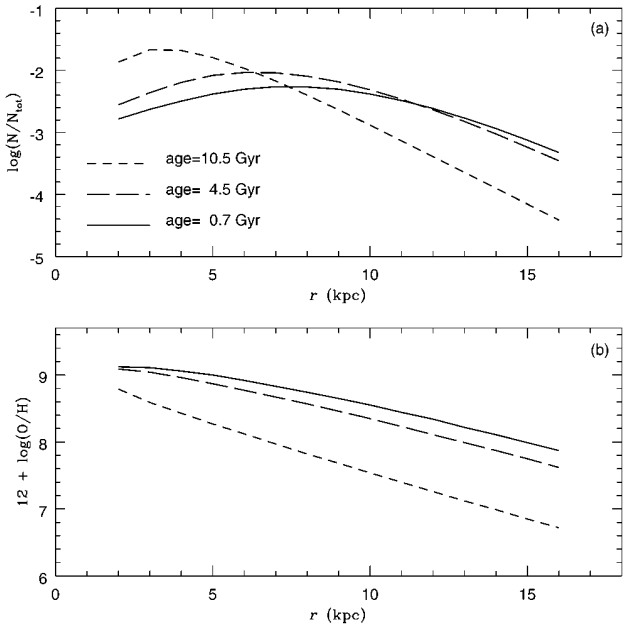

FIG. 2.—Evolution, at three different ages, of the radial distribution of (*a*) normalized number of progenitors of present-day PNs and (*b*) oxygen abundance relative to hydrogen.

assumed dependency of the star formation rate. In consequence, saturation is quickly reached at the central parts, flattening the O/H and PNPs gradients with time.

3. DYNAMICAL EVOLUTION

To model the evolution with time of the space distribution and the kinematic properties of the populations of stars that, after a given time, become PNs, we chose the following approach.

A large number of perturbed Galactic orbits was numerically integrated using the Galactic potential of Allen & Santillán (1991). We modeled the perturbations caused by encounters with density inhomogeneities in the Galactic disk (spiral arms, giant molecular clouds, or cloud complexes, etc.) by subjecting each star to velocity perturbations of random direction and of a magnitude of 0.78 km s^{-1}, each million years spent within the Galactic disk ($|z| < 500$ pc). As shown by Wielen (1977), the orbital diffusion caused by such perturbations accurately accounts for the observed increase with age of the stellar velocity dispersions. We have checked the validity of the parameters derived by Wielen for his force-free diffusion model, in particular, the diffusion coefficient, using more recent data obtained by Edvardsson et al. (1993). The results differ very little from those obtained by Wielen (Allen 1997).

In each numerical experiment we included a total of 1350 stars, situated on the Galactic plane and distributed in 15 rings with radii centered at $r = 2, 3, \ldots, 16$ kpc. Each ring thus comprised 90 stars. We assumed the initial space velocities to have random directions and random magnitudes, with a total dispersion of 10 km s^{-1} with respect to the local circular velocity. Each experiment was run for a time corresponding to the time it takes for stars of a given mass to reach the planetary nebula stage. A total of 16 experiments were performed with final times ranging from 0.1 to 12.8 Gyr, an interval that corresponds to planetary nebula progenitors with initial masses from 8.41–0.83 $M_\odot$. At the end of each numerical experiment we computed averages and dispersions for the radial distances, the distances from the Galactic plane, and the three space velocity components.

The main results of the dynamical model are summarized in Tables 2 and 3. In Table 2 we show the mean orbital parameters obtained at the end of the integrations for three representative Galactocentric radii. The first column lists the ages of the objects. The next columns list the mean Galactocentric distance $\langle r \rangle$, the mean distance above or below the Galactic plane $\langle |z| \rangle$, the mean space velocity relative to the local circular velocity $\langle v \rangle$, and the total velocity dispersion σ_v. Units for $\langle r \rangle$ and $\langle |z| \rangle$ are kpc and for $\langle v \rangle$ and for σ_v are km s^{-1}. In Table 3 we list again the ages of the objects in the first column. In the next columns we display, for three representative Galactocentric radii, the percentage of the total number of stars that have total space velocities (relative to the local circular velocity) exceeding 60 or 70 km s^{-1}. These fractions are useful to compare the results of the dynamical model with observational data on planetary nebulae.

TABLE 2

MEAN ORBITAL PARAMETERS FOR THREE GALACTIC RINGS

	$r = 7$ kpc				$r = 8$ kpc				$r = 9$ kpc			
AGE (Gyr)	$\langle r \rangle$ (kpc)	$\langle \lvert z \rvert \rangle$ (kpc)	$\langle v \rangle$ (km s^{-1})	σ_v (km s^{-1})	$\langle r \rangle$ (kpc)	$\langle \lvert z \rvert \rangle$ (kpc)	$\langle v \rangle$ (km s^{-1})	σ_v (km s^{-1})	$\langle r \rangle$ (kpc)	$\langle \lvert z \rvert \rangle$ (kpc)	$\langle v \rangle$ (km s^{-1})	σ_v (km s^{-1})
12.8.....	7.751	0.388	68.14	72.97	8.974	0.466	67.80	71.15	10.046	0.487	66.58	74.41
12.3.....	7.762	9.383	68.27	71.23	8.826	0.437	69.09	73.95	9.586	0.505	62.82	67.64
11.5.....	7.230	0.305	62.56	67.72	8.348	0.329	68.36	74.70	9.836	0.461	58.52	63.43
10.5.....	7.576	0.353	64.27	67.78	9.109	0.385	64.09	68.05	10.379	0.468	63.61	68.36
9.5.....	7.717	0.296	59.78	63.66	8.760	0.329	58.45	63.34	9.478	0.430	61.16	65.96
8.5.....	7.442	0.270	57.83	64.32	8.762	0.364	61.33	65.32	9.739	0.402	58.95	64.11
7.5.....	7.511	0.235	55.15	58.70	8.352	0.328	53.69	58.91	9.561	0.326	55.21	58.87
6.5.....	7.422	0.240	53.31	56.43	8.293	0.284	48.48	52.35	9.468	0.309	53.08	56.94
5.5.....	7.428	0.184	46.82	50.31	8.415	0.240	48.63	54.13	9.390	0.268	51.46	55.48
4.5.....	7.293	0.187	46.45	51.07	8.491	0.247	44.78	47.26	9.243	0.250	45.87	48.71
3.5.....	7.168	0.145	40.39	44.01	8.647	0.179	41.14	43.82	9.363	0.222	39.63	43.82
2.5.....	7.040	0.150	34.78	38.26	8.195	0.145	33.50	36.45	9.251	0.170	32.76	35.76
1.5.....	7.102	0.102	26.71	28.72	7.945	0.120	24.98	27.19	9.112	0.136	27.63	30.56
0.7.....	6.947	0.069	20.63	22.73	7.997	0.089	19.01	20.36	8.980	0.103	20.19	21.90
0.3.....	7.054	0.057	13.55	14.50	8.069	0.060	13.68	15.30	9.141	0.075	15.61	16.53
0.1.....	6.969	0.034	11.22	12.29	8.010	0.047	10.64	11.44	8.995	0.049	10.29	11.27

TABLE 3

FRACTION OF STARS WITH HIGH VELOCITIES

	$r = 7$ kpc		$r = 8$ kpc		$r = 9$ kpc	
AGE (Gyr)	>60 km s^{-1} (%)	>70 km s^{-1} (%)	>60 km s^{-1} (%)	>70 km s^{-1} (%)	>60 km s^{-1} (%)	>70 km s^{-1} (%)
12.8.....	59	56	57	48	52	38
12.3.....	59	41	59	44	48	34
11.5.....	53	38	50	38	41	31
10.5.....	58	33	48	34	48	36
9.5.....	43	32	47	28	46	31
8.5.....	42	31	46	34	42	22
7.5.....	38	23	38	24	36	22
6.5.....	32	22	26	14	32	20
5.5.....	27	13	31	18	34	23
4.5.....	27	17	23	12	21	9
8.5.....	14	7	14	7	18	5
2.5.....	8	1	5	2	4	1
1.5.....	0	0	0	0	0	0

In Figure 3 we plot averages for each Galactic ring of the height, above or below the plane, reached by PN progenitors as a result of dynamical evolution. Figure 3 clearly shows the increase with age of $\langle |z| \rangle$, the average heights attained. Also strikingly evident in this figure is the ever greater spread of $\langle |z| \rangle$ as we go to larger Galactocentric radii.

4. DISCUSSION

4.1. *PN Lifetimes*

To compare our model with observations, we will assume that the lifetimes for detection of PNs of different types are similar. In what follows we will explore this assumption.

The observable time of a PN is given by

$$t = \frac{(R_f - R_i)}{\langle V \rangle}, \tag{3}$$

where R is the radius of the nebula and $\langle V \rangle$ the average velocity of expansion from R_i to R_f. In the optically thick (ionization bounded) phase, $\langle V \rangle$ denotes the average velocity of the ionization front relative to the central star, $V_{\rm ion}$, while in the optically thin (matter bounded) phase $\langle V \rangle$ denotes the average velocity of expansion of matter, $V_{\rm exp}$, given by the Doppler effect.

Usually we will be able to determine the abundances of PNs with an emission measure, EM, higher than a certain threshold value, and since $\mathrm{EM} = \int N_e^2\, dr \propto M^2 R^{-5}$, it follows that when comparing two PNs,

$$\frac{R_1}{R_2} = \left(\frac{M_1}{M_2}\right)^{2/5}, \tag{4}$$

where M is the ionized mass of each object. By combining equations (3) and (4), it follows that the relative time of visibility of two PNs will be given by

$$\frac{t_1}{t_2} = \left(\frac{M_1}{M_2}\right)^{2/5} \frac{\langle V_2 \rangle}{\langle V_1 \rangle}. \tag{5}$$

Marten, Gesicki, & Szczerba (1993) find that for an optically thick model of a PN $V_{\rm ion}/V_{\rm exp} \sim 1.3$. PNs are expected to have an optically thick phase followed by an optically thin phase; moreover, Mallik & Peimbert (1988) find that most of the objects in their PNs sample are optically thick in at least some directions, while Méndez, Kudritzki, & Herrero (1992) conclude that most of the objects in their PNs sample are optically thin in at least some directions. Consequently, a large fraction of PNs are optically thick in some directions and optically thin in others. From the previous arguments we conclude that $\langle V_{\rm exp\,2} \rangle / \langle V_{\rm exp\,1} \rangle$ provides us with a good approximation to $\langle V_2 \rangle / \langle V_1 \rangle$ in equation (5).

When comparing large PNs, those near the EM threshold value to derive chemical abundances, it is found that PNs of type I have ionized masses about a factor of 2 higher than those of type II and about 5 times higher than those of type III; on the other hand, their $V_{\rm exp}$ are about 35 km s^{-1} for type I, 25 km s^{-1} for type II, and 20 km s^{-1} for type III (e.g., Dopita 1993, 1997). Moreover, K648, the type IV PN in the globular cluster M15, shows a $V_{\rm exp} \leq 17$ km s^{-1}, in agreement with the previous trend (G. H. Herbig 1972, private communication). Consequently, by comparing lifetimes by means of equation (5), it is found that the change in mass is compensated by the change in $V_{\rm exp}$.

Two of the largest type I PNs with accurate abundances are NGC 7293 and ESO 166-PN21 (Peimbert & Torres-Peimbert 1987; Peña et al. 1997); they have R values of about 0.5 pc. These examples imply that it is possible to obtain accurate abundances of type I PNs with $R \leq 0.6$ pc. On the other hand, one of the largest type IV PN with accurate abundances is NGC 4361, with an R value of 0.24 pc and an ionized mass of 0.07 $M_\odot$ (Torres-Peimbert, Peimbert, & Peña 1990). From this example it is found that it is

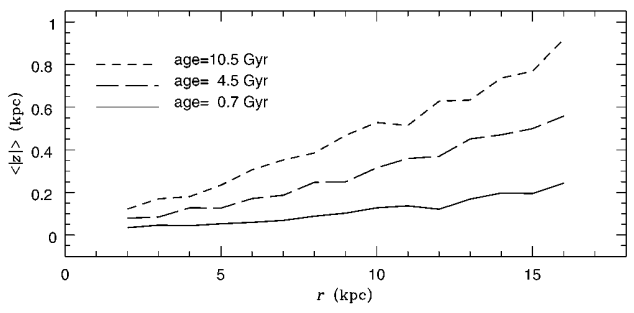

FIG. 3.—Mean distances to the Galactic plane reached by PN progenitors of three different ages, averaged over the objects of each ring, as a function of Galactocentric radius.

possible to obtain accurate abundances for an object with $M = 0.07\ M_\odot$ and $R \sim 0.3$ pc, in agreement with the discussion in the previous paragraph. Typical large type II and III PNs (those in the optically thin stage) have masses around $0.2\ M_\odot$; therefore, only those PNs with ionized masses smaller than $0.02\ M_\odot$ will have lifetimes 40% smaller than those of typical PNs.

4.2. *Radial Gradients*

In Figures 4, 5, and 6 we compare the gradients predicted by our model with those derived from observations by Maciel & Köppen (1994). To make this comparison we will assume that there are no selection effects in the sample and that there are no systematic errors in the distance or abundance determinations. We will get back to these assumptions later on. We will also assume that the lifetimes of PNs of different types are similar.

In Figure 4 we have assumed that (*a*) all IMSs become PNs, (b) the types of PNs depend only on the initial mass of the parent star, and (*c*) the fraction of each type is similar to those given by the percentages observed by Maciel & Köppen (1994). The fit is very poor in the sense that the observed abundances for types II and III PNs are considerably higher than the predicted ones.

In Figure 5 we have made the following assumptions: (*a*) all IMSs become PNs, (*b*) all type I PNs have progenitors with masses higher than $2.02\ M_\odot$ in the main sequence, (*c*) all progenitors with less than $2.02\ M_\odot$ in the main sequence and with peculiar velocities smaller than 60 km s^{-1} produce type II PNs, and (*d*) all progenitors with less than $2.02\ M_\odot$ in the main sequence and peculiar velocities higher than 60 km s^{-1} produce type III PNs. The fit to the gradients is significantly better than in Figure 4. The main problem is that the predicted fraction of type III PNs is considerably higher than observed.

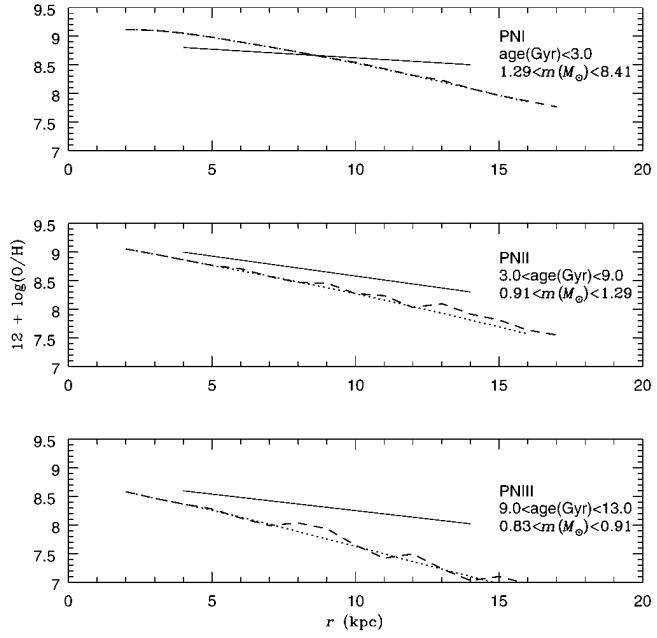

FIG. 4.—O/H radial gradients for PNs of types I, II, and III. The solid lines show the gradients derived by Maciel & Köppen (1994). Dashed lines and dotted lines present the model predictions with and without dynamical effects, respectively. The age and the mass range of PNs progenitors are indicated. The percentage of objects in each panel are 30%, 49%, and 21% for types I, II, and III, respectively. These percentages are similar to the observed ones.

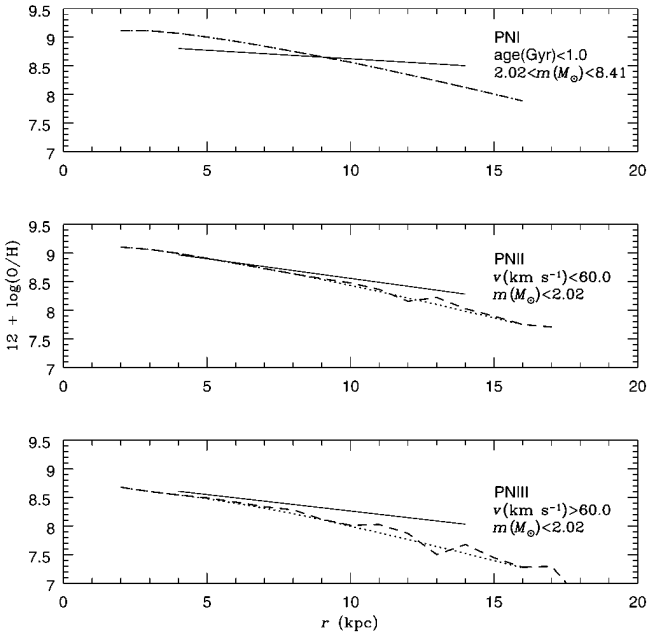

FIG. 5.—Same as Fig. 4, but for a different definition of the types. Also, the mass limits are different, and the separation between types II and III is based on the peculiar velocity and not on the mass of the progenitor. In this figure the percentages are 13%, 42%, and 45% for types I, II, and III, respectively. This fit to the gradients is better than that of Fig. 4, but the percentages do not agree with the observed ones.

We have assumed that type III PNs are those with a *computed peculiar velocity* higher than 60 km s^{-1}, while Peimbert (1978) and Maciel & Köppen (1994) have assumed that type III PNs are those with an *observed peculiar radial velocity* higher than 60 km s^{-1}. Considering the errors in the distance determinations, probably both definitions include a substantial amount of objects in common.

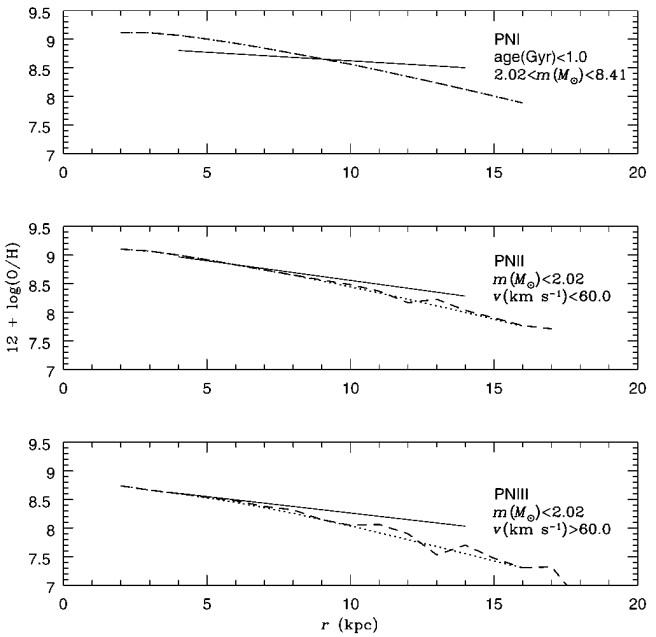

FIG. 6.—Same as Fig. 5, but assuming that not all low IMSs produce PNs (see Table 4 and the discussion in the text). The percentages are 30%, 44%, and 26% for types I, II, and III, respectively. We consider the fit to the gradients of type II and III PNs to be as good as that obtained for the H II regions. Moreover, the percentages of the three types of PNs are similar to those observed.

In Figure 6 we have assumed the same mass for the progenitors and the same velocity boundaries for the different types of PNs as in Figure 5, but that only about half of the IMSs produce PNs. This assumption was made to be able to reproduce the observed percentages of types I, II, and III by Maciel & Köppen (1994). The fraction of IMSs that produce PNs for a given mass of the progenitor star, $m(M_\odot)$, is given by the fraction function (FF) defined in Table 4. We have taken into account the FF to produce Figure 6. We consider Figure 6 to be a reasonable fit to the observational data.

The average fraction of IMSs that become PNs given by the FF and our chemodynamical model amounts to 43%, 47%, and 52% for those objects in the 7, 8, and 9 kpc rings, respectively. The average fraction not only reproduces the relative numbers of PNs of different types, but it is also in agreement with the PNs birth rate per unit luminosity, $\dot{\xi}$ (see § 4.6), and with the fraction of white dwarfs with masses equal or higher than 0.55 $M_\odot$ (see § 4.7). We have suggested an FF that decreases with mass for the following reasons: (*a*) the predicted scale height is higher than observed (see § 4.4), (*b*) the PNs birth rate in extragalactic systems decreases monotonically with $(B-V)_0$ and with $M_{\rm bol}$ (see § 4.6), and (*c*) white dwarfs with nuclei smaller than 0.55 $M_\odot$ are expected to come from the low-mass end of the initial mass function (see § 4.7). Furthermore, we did not adopt a step function given by a limiting initial mass below which no PNs is formed because there are a few halo planetary nebulae (type IV; e.g., Peimbert 1992) whose progenitors are very low mass stars.

In Table 5 (see also Fig. 6) we present the gradients derived from our model after applying the FF, as well as from observations (Maciel & Köppen 1994). In the first line, labeled "CM," we present the predicted gradients from Galactic chemical evolution only, without considering the stellar dynamical effects. In the second line, labeled "CDM," we present the predicted gradients from the Galactic chemical evolution and the stellar dynamical evolution. It is clear from this table that the predicted radial gradients are almost independent of the stellar dynamical effects. The observed absolute abundances in the solar neighborhood are in good agreement with the predicted ones. On the other hand the observed gradients are smaller than the predicted ones by factors of 3.1, 1.3, and 2.0 for types I, II, and III, respectively. We consider that most of the discrepancy is due to two different effects: errors in the distances and errors in the abundance determinations.

TABLE 4

FRACTION FUNCTION (FF)[a]

$m(M_\odot)$	FF
0.833–0.840	0.10
0.840–0.850	0.12
0.850–0.869	0.14
0.869–0.890	0.16
0.890–0.914	0.18
0.914–0.942	0.21
0.942–0.975	0.24
0.975–1.018	0.27
1.018–1.080	0.40
1.080–1.167	0.45
1.167–1.292	0.50
1.292–1.481	0.55
1.481–2.023	0.60
2.023–8.406	1.00

[a] Fraction of stars that produce a visible PN during their evolution.

TABLE 5

PN RADIAL ABUNDANCE GRADIENTS[a] EVALUATED AT THE SOLAR NEIGHBORHOOD

	TYPE I		TYPE II		TYPE III	
PARAMETER	*a*	*b*	*a*	*b*	*a*	*b*
CM[b]	−0.092	8.75	−0.095	8.65	−0.104	8.26
CDM[c]	−0.092	8.75	−0.088	8.65	−0.114	8.32
Observed[d]	−0.030	8.68	−0.069	8.70	−0.058	8.38
Error (±)[d]	0.007	0.06	0.006	0.05	0.008	0.06

[a] $12 + \log(\mathrm{O/H}) = a(r - 8\ \mathrm{kpc}) + b$, where *a* is in dex kpc^{-1} and *b* is in dex.
[b] Chemical model.
[c] Chemodynamical model.
[d] Maciel & Köppen 1994.

Terzian (1993) has presented a review on distances to planetary nebulae not based on statistical methods, which are in principle the best distances available for Galactic planetary nebulae, and finds that distances derived by different authors vary for the same object by factors of 2 or 3, or even more in some cases. By assuming a random error of a factor of 2 in the distances, it is found that the derived average distance is a factor of 1.25 higher than the real one and, consequently, that the observed gradients become 1.25 times smaller than the real ones. If the random error amounts to a factor of 3, the derived average distance becomes 1.67 larger than the real one.

Type I PNs present larger temperature fluctuations than other types of PNs (Peimbert, Torres-Peimbert, & Luridiana 1995) that often are not taken into account to derive the chemical composition of these objects (Peimbert, Luridiana, & Torres-Peimbert 1995). If this effect is considered, the O/H values become larger. Moreover, this effect is expected to be larger for PNs at smaller Galactocentric distances, because the higher the O/H values the lower the electron temperature and the more sensitive the O/H determination to the adopted electron temperature.

4.3. *Variation of the Radial Gradients with Time*

The temporal evolution on the chemical radial distribution of the Galactic disk has been considered an important issue in the most recent and detailed chemical evolution models (see Tosi 1996, and Maciel 1996, 1997, for interesting reviews). Therefore, we will discuss the behavior of the gradients as a function of time predicted by our model.

In § 2 we showed and discussed our predicted O/H gradients in the interstellar medium at three different ages. At the solar distance the O/H gradient amounts to −0.09, −0.11, and −0.15 dex kpc^{-1} for ages of 0.7, 4.5, and 10.5 Gyr, respectively, which implies that the interstellar medium gradient flattens with time. In this respect our model agrees with those of Ferrini et al. (1994) and Mollá, Ferrini, & Díaz (1997), since they also predict a flattening of the interstellar medium abundance gradients with time, and disagrees with those of Tosi (1988) and Chiappini, Matteucci, & Gratton (1996), which predict the opposite.

Alternatively, the O/H gradients derived from our model for types III, II, and I amount to −0.11, −0.09, and −0.09 dex kpc^{-1}, respectively. The flattening of the gradient from type III to type I PNs is considerably smaller than that of the interstellar medium in the last 10.5 Gyr; the difference is

due to the convolution of the star formation rate with the range of masses involved in each PN's type.

From observations Maciel & Köppen (1994) found that abundance gradients become steeper along the sequence of type I-II-III PNs, for O and flatter for S and Ar. We consider that the differences among the three elements are due to observational errors, and since we expect these elements to behave similarly, an average of the three might be more representative; this average amounts to -0.055, -0.062, and -0.052 dex kpc^{-1} for types I, II, and III, respectively.

We consider that at present the observational determinations are not good enough to conclude whether the gradients flatten or steepen with time. From our model the interstellar medium gradients flatten with time, but the PN ones are almost constant with time. We need higher quality observations to use the variation of the gradients with time as a strong constraint for modeling the chemical evolution of the Galactic disk.

4.4. *PN Scale Heights*

From observations the following scale heights are derived for PNs: 90 pc (Cahn & Kaler 1971), 100 pc (Ishida & Weinberger 1987), 115 pc (Cahn & Wyatt 1976), 125 pc (Daub 1982), 130 pc (Amnuel et al. 1984), and 153 pc (Mallik 1991). These values are based on different data sets and different distance scales. In general, as expected, the larger the distance scale adopted the larger the derived scale height (Peimbert 1993).

Table 6 presents the scale heights predicted by our chemodynamical model for the solar neighborhood, as well as the observational value derived by Mallik (1991). It will be very important to derive observed scale heights from complete samples of type I and types II + III independently. From our model, and under the assumption that all IMSs produce PNs, it is found that the PNs scale height in the solar neighborhood amounts to 218 pc (see Table 6). This value is considerably higher than the observed ones and implies that not all the IMSs with small masses produce PNs, in agreement with the results obtained in § 4.2. Alternatively, the scale height derived by assuming that only the fraction of IMSs given by the FF presented in Table 4 produce PNs amounts to 164 pc, in good agreement with the scale height derived by Mallik (1991).

The adoption of a distance scale considerably shorter than that adopted by Mallik (1991) would yield PN birth rates larger than predicted (Peimbert 1993).

4.5. *Vertical Gradients*

In Figure 7 we present the O/H vertical distributions derived from our model for three Galactocentric distances. Notice that the gradients become flatter at higher Galactocentric distances due to the increase of $\langle |z| \rangle$ with r. In Table 7 we present the vertical O/H gradients for three combinations of PNs types assuming that all IMSs produce PNs and that only the fraction given by the FF produce PNs; the values in this table correspond to the distributions plotted in Figure 7.

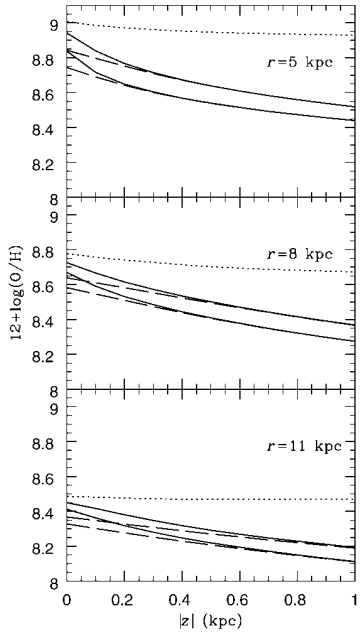

FIG. 7.—O/H vertical gradients. In each panel the upper curve corresponds to type I PNs. The lower full line corresponds to the case when all IMSs produce PNs, and includes types I + II + III. The upper full line only includes the PNs of types I + II + III given by the FF (see Table 4). The dashed lines include only PNs of types II + III for each case.

From observational data Köppen & Cuisinier (1997) have computed O/H, S/H, and Ar/H vertical gradients that amount to -0.055, -0.11, and -0.15 dex kpc^{-1}, respectively. From observations of H II regions in the Galaxy and other galaxies we expect the three gradients to be similar; therefore, we conclude that a gradient of -0.10 dex kpc^{-1} is typical from their data. Such value is about a factor of 3 smaller than those derived for types I + II + III from our model.

The gradients derived from our model and from these observations are not expected to be the same for the following reasons: (*a*) the observations include objects with projected distances from the Sun of 5.0 kpc or less, and the observed gradients were derived under the assumption that the vertical gradients were independent of Galactocentric distance; on the other hand, our model predicts different

TABLE 6

SCALE HEIGHTS FROM PNs IN THE SOLAR NEIGHBORHOOD[a]

Parameter	Type I	Types I + II + III	Types II + III
CDM[b]	69	218	243
CDM[c]	69	164	208
Observed[d]	...	153	...

[a] The scale heights, in parsecs, correspond to averages for $r = 7$, 8, and 9 kpc; they were derived from the data presented in Tables 1 and 2.

[b] Assuming that all IMSs produce a PN.

[c] Assuming that only a fraction of IMSs produce PNs; the fractions are those of Table 4.

[d] From Mallik 1991.

TABLE 7

VERTICAL O/H GRADIENTS[a]

	r (kpc)		
PN	4, 5, 6	7, 8, 9	10, 11, 12
Type I:			
All	-0.078	-0.103	-0.015
Type I + II + III:			
All	-0.399	-0.395	-0.299
All × FF	-0.423	-0.358	-0.256
Type II + III:			
All	-0.305	-0.309	-0.216
All × FF	-0.325	-0.270	-0.177

[a] In dex kpc^{-1}.

scale heights and different vertical gradients as a function of Galactocentric distance (see Fig. 3 and Tables 2 and 7); (*b*) the scale height of our sample (after taking into account the FF) is of 164 pc, while the observed sample has a scale height of about 550 pc; the difference is due to an observational selection effect mainly caused by extinction in the plane of the Galaxy; and (*c*) errors in the adopted distance for each object and in the abundance determinations tend to reduce the value of the derived gradients. It is beyond the scope of this paper to make a more detailed comparison with observations. An unbiased complete sample of PNs in the solar neighborhood is needed to advance in this comparison.

4.6. *PNs Birth Rates*

Renzini & Buzzoni (1986) found that the stellar death rate per solar bolometric luminosity, $\dot{S}(t_1)$, is almost independent of the initial mass function adopted, for galaxy models of age t_1 and a single burst of star formation. Peimbert (1990b) has shown that to a very good approximation $\dot{S}(t_1)$, for $t_1 > 1$ Gyr, corresponds to the stellar death rate per unit luminosity for systems with a constant rate of star formation and for systems with a decreasing rate of star formation. This result is very powerful and implies that galaxies where star formation started more than 1 Gyr years ago and that are not suffering from a extreme burst of star formation, $\dot{S}(10^{-12}\ \mathrm{yr}^{-1}\ L_{\odot}^{-1})$ should be in the 18–22 range. Under the assumption that all IMSs become PNs, it follows that the stellar death rate is almost equal to the PNs birth rate.

Peimbert (1990b) found a decrease of the PNs birth rate per unit luminosity, $\dot{\xi}$ with M_{bol} and $(B-V)_0$ for extragalactic systems. The $\dot{\xi}$ value decreases from about 15 to about 2.7 in units of $10^{-12}\ \mathrm{yr}^{-1}\ L_{\odot}$; these values imply that not all IMSs produce PNs. Moreover, since the average age of the stellar content increases with M_{bol} and $(B-V)_0$, these $\dot{\xi}$ values imply that the fraction of IMSs that produce PNs decreases with the decreasing mass of their progenitors.

By comparing the M_{bol} and the $(B-V)_0$ value of the Galaxy with the M_{bol} versus $\dot{\xi}$ and $(B-V)_0$ versus $\dot{\xi}$ relations for extragalactic systems, it is found that $\dot{\xi} = 9 \pm 3 \times 10^{-12}\ \mathrm{yr}^{-1}\ L_{\odot}^{-1}$ (Peimbert 1993). This result is in fair agreement with the $\dot{\xi}$ values derived from (*a*) the surface density of PNs and the surface brightness at the solar Galactocentric distance and (*b*) the local density of PNs and the solar neighborhood luminosity function (Peimbert 1993 and references therein). Moreover, this value of $\dot{\xi}$ implies that in the solar neighborhood about half of the IMSs go through the PNs stage, in agreement with the results presented in § 4.2.

4.7. *PNs and White Dwarfs*

The white dwarf birth rate estimated by Weidemann (1991) of $20 \times 10^{-12}\ \mathrm{yr}^{-1}\ L_{\odot}^{-1}$ is in agreement with the death rate estimated in § 4.6 for IMSs, and it is a factor of 2.2 higher than the estimated PNs death rate.

Stasinska, Gorny, & Tylenda (1997) have determined the masses of 125 PN central stars; all of them have masses higher than 0.55 $M_{\odot}$. Their sample does not include known close binaries nor stars with H-poor atmospheres. Alternatively, Bergeron, Saffer, & Liebert (1992), and Bragaglia, Renzini, & Bergeron (1995) have determined the masses of 164 white dwarfs divided as follows: 9% have masses smaller than 0.4 $M_{\odot}$, 48% between 0.4 $M_{\odot}$ and 0.55 $M_{\odot}$, and 43% masses higher than 0.55 $M_{\odot}$. According to these authors, the objects with masses smaller than 0.4 $M_{\odot}$ are helium white dwarfs, the outcome of close binary evolution.

It is reasonable to associate white dwarfs with masses higher than 0.55 $M_{\odot}$ with those stars that produced PNs, and white dwarfs in the 0.4–0.55 $M_{\odot}$ range with those that did not produce PNs. The failure to produce a PN could have been due to a very slow rate of post–asymptotic giant branch (AGB) evolution (those with masses in the 0.51–0.55 $M_{\odot}$ range; see Weidemann & Koester 1983 and references therein) or because stars with masses smaller than 0.51 $M_{\odot}$ do not reach the AGB at all, but stay at lower luminosities and evolve toward the white dwarf stage without PN ejection (Sweigart, Mengel, & Demarque 1974). Weidemann & Koester (1983) already suggested that the fraction of white dwarfs not going through PN stages might be as high as 50%.

5. SUMMARY

Accurate radial gradients test mainly the chemical evolution part of our model, while vertical gradients test both the chemical and the dynamical evolution parts. The dynamical evolution produces a small increase with time of the average Galactocentric distance. This increase produces negligible changes between the observed radial gradients and the initial radial gradients provided by the chemical evolution model for ages smaller than 7 Gyr. The radial gradients for stellar populations older than 7 Gyr become marginally flatter.

Under the assumption that all intermediate mass stars [those with $0.83 < m(M_{\odot}) < 8.4$] become PNs, it is not possible to adjust the observed radial gradient of type III PNs nor the absolute value of O/H in the solar neighborhood.

We find evidence that not all IMSs go through the PN stage, and we have defined a fraction function, FF, presented in Table 4, which gives us the fraction as a function of mass of those IMSs that do go through the PNs stage. Our FF is in qualitative agreement with (*a*) the O/H value for type III PNs of the solar neighborhood predicted by our model, (*b*) the scale height of PNs in the solar neighborhood, (*c*) the estimated PNs birth rate for the solar neighborhood, (*d*) the decrease of the PNs birthrate with M_{bol} and $(B-V)_0$ in extragalactic systems, and (*e*) with the fraction of white dwarfs with masses in the 0.4–0.55 $M_{\odot}$ range that presumably did not go through the PN stage.

The predicted peculiar radial velocities are smaller than the observed ones, which implies that errors in the adopted distances increase the observed peculiar velocities. The observed type III PNs gradient is compared with that produced by those stars with progenitor masses in the 0.83–2.02 $M_{\odot}$ range and peculiar spatial velocities larger than 60 km s^{-1}, while the observed type II PNs gradient is compared with that produced by the stars in the same mass range and peculiar spatial velocities smaller than 60 km s^{-1}.

An excellent fit to the abundances at the solar Galactocentric distance is obtained for the PNs of the three types; these fits are independent of the distances adopted to the PNs. The observed radial gradient for type II PNs is in good agreement with that predicted from our model; we consider that this is the best observed gradient because in general the abundance and distance determinations of type II PNs are of higher quality than those of PNs of types I and III.

The fit for the radial gradient derived from type I PNs is poor. We argue that this is mainly due to the presence of temperature fluctuations that have not been taken into account in the abundance determinations. The predicted gradient changes very little if the low mass end of type I PNs is changed from 1.3 to 2.5 $M_{\odot}$.

The O/H radial gradient in the interstellar medium predicted by the chemical part of our model flattens with time as the Galaxy evolves. On the other hand, the O/H gradients derived from our model for type I and type II PNs are practically the same, while that derived for type III PNs is only slightly steeper. This is mainly due to three causes: (*a*) the combination of progenitor stars of different masses in each type; (*b*) the effect of the FF, which reduces the fraction of small mass stars that produce PNs; and (*c*) the fact that at low Galactocentric distances the number of predicted PNs increases with the age of the progenitor star, while at large Galactocentric distances the opposite is true.

The radial gradient fits for Galactocentric distances larger than about 11 kpc are only fair, in the sense that the abundances are smaller than observed. The same situation is present when comparing the model abundance gradients with those derived from Galactic H II regions. These comparisons imply that the chemical evolution model has to be modified to produce a better fit at larger Galactocentric distances.

REFERENCES

Allen, C. 1998, in preparation
Allen, C., & Santillán, A. 1991, Rev. Mexicana Astron. Astrofis., 22, 255
Amnuel, P. R., Guseinov, O. H., Novruzova, H. I., & Rustamov, Yu. S. 1984, Ap&SS, 107, 19
Bergeron, P., Saffer, R. A., & Liebert, J. 1992, ApJ, 394, 228
Bragaglia, A., Renzini, A., & Bergeron, P. 1995, ApJ, 443, 735
Cahn, J. H., & Kaler, J. B. 1971, ApJS, 22, 319
Cahn, J. H., & Wyatt, S. P. 1976, ApJ, 210, 508
Carigi, L. 1996, Rev. Mexicana Astron. Astrofis., 32, 179
Charbonnel, C., Meynet, G., Maeder, A., & Schaerer, D. 1996, A&AS, 115, 339
Chiappini, C., Matteucci, F., & Gratton, R. 1996, ApJ, 477, 765
Dame, T. M. 1993, in AIP Conf. Proc. 278, Back to the Galaxy, ed. S. Holt & F. Verter (New York: AIP), 267
Daub, C. T. 1982, ApJ, 260, 612
Dopita, M. A. 1993, in IAU Symp. 155, Planetary Nebulae, ed. R. Weinberger & A. Acker (Dordrecht: Kluwer), 439
———. 1997, in IAU Symp. 180, Planetary Nebulae, ed. H. J. Habing & H. J. G. L. M. Lamer (Dordrecht: Kluwer), in press
Edvardsson, B., Andersen, J., Gustafsson, B., Lambert, D. L., Nissen, P. E., & Tomkin, J. 1993, A&A, 275, 101
Ferrini, F., Mollá, M., Pardi, M. C., & Díaz, A. I. 1994, ApJ, 427, 745
Gilmore, G. 1989, in The Milky Way as a Galaxy, ed. R. Buser & I. King (Geneva: Geneva Obs.), 36
Ishida, K., & Weinberger, R. 1987, A&A, 178, 227
Köppen, J., & Cuisinier, F. 1997, A&A, 319, 98
Kroupa, P. Tout, C. A., & Gilmore, G. 1993, MNRAS, 262, 545
Kuijken, K., & Gilmore, G. 1989, MNRAS, 239, 605
———. 1991, ApJ, 367, L9
Lacey, C. G., & Fall, S. M. 1985, ApJ, 290, 154
Maciel, W. J. 1996, in Stellar Abundances, ed. B. Barbuy, W. J. Maciel, & J. C. Gregorio-Hetem (São Paulo: Universidade de São Paulo/IAG), 79
———. 1997, in IAU Symp. 180, Planetary Nebulae, ed. H. J. Habing & H. J. G. L. M. Lamers (Dordrecht: Kluwer), in press
Maciel, W. J., & Köppen, J. 1994, A&A, 282, 436
Mallik, D. C. V. 1991, Proc. Astron. Soc. Australia, 9, 15
Mallik, D. C. V., & Peimbert, M. 1988, Rev. Mexicana Astron. Astrofis., 16, 111
Marten, H., Gesicki, K., & Szczerba, R. 1993, in IAU Symp. 155, Planetary Nebulae, ed. R. Weinberger & A. Acker (Dordrecht: Kluwer), 523
Méndez, R. H., Kudritzki, R. P., & Herrero, A. 1992, A&A, 260, 329
Mollá, M., Ferrini, F., & Díaz, A. I. 1997, ApJ, 475, 519
Peimbert, M. 1978, in IAU Symp. 103, Planetary Nebulae: Observations and Theory, ed. Y. Terzian (Dordrecht: Reidel), 215
———. 1979, in The Large Scale Characteristics of the Galaxy, ed. W. B. Burton (Dordrecht: Reidel), 307
Peimbert, M. 1990a, Rep. Prog. Phys., 53, 1559
———. 1990b, Rev. Mexicana Astron. Astrofis., 20, 119
———. 1992, in Elements and the Cosmos, ed. M. G. Edmunds & R. J. Terlevich (Cambridge: Cambridge Univ. Press), 196
———. 1993, in IAU Symp. 155, Planetary Nebulae, ed. R. Weinberger & A. Acker (Dordrecht: Kluwer), 523
Peimbert, M., Luridiana, V., & Torres-Peimbert, S. 1995, Rev. Mexicana Astron. Astrofis., 31, 147
Peimbert, M., & Torres-Peimbert, S. 1987, Rev. Mexicana Astron. Astrofis., 14, 540
Peimbert, M., Torres-Peimbert, S., & Luridiana, V. 1995, Rev. Mexicana Astron. Astrofis., 31, 131
Peña, M., Ruiz, M. T., Bergeron, P., Torres-Peimbert, S., & Heathcote, S. 1997, A&A, 317, 911
Prantzos, N., & Aubert, O. 1995, A&A, 302, 69
Rana, N. C. 1991, ARA&A, 29, 129
Rana, N. C., & Basu, S. 1992, A&A, 265, 499
Renzini, A., & Buzzoni, A. 1986, in Spectral Evolution of Galaxies, ed. C. Chiosi & A. Renzini (Dordrecht: Reidel), 195
Renzini, A., & Voli, M. 1981, A&A, 94, 175
Rocha-Pinto, H. J., & Maciel, W. J. 1996, MNRAS, 279, 447
Schaller, G., Schaerer, D., Meynet, G., & Maeder, A. 1992, A&ASS, 96, 269
Shaver, P. A., McGee, R. X., Newton, L. M., Danks, A. C., & Pottasch, S. R. 1983, MNRAS, 204, 53
Stasinska, G., Gorny, S. K., & Tylenda, R. 1997, A&A, 327, 736
Sweigart, A. V., Mengel, J. G., & Demarque, P. 1974, A&A, 30, 13
Terzian, Y. 1993, in IAU Symp. 155, Planetary Nebulae, ed. R. Weinberger & A. Acker (Dordrecht: Kluwer), 109
Torres-Peimbert, S., & Peimbert, M. 1997, in IAU Symp. 180, Planetary Nebulae, ed. H. J. Habing & H. J. G. L. M. Lamers (Dordrecht: Kluwer), in press
Torres-Peimbert, S., Peimbert, M., & Peña, M. 1990, A&A, 233, 540
Tosi, M. 1988, A&A 197, 33
———. 1996, ASP Conf. Ser. 98, From Stars to Galaxies: The Impact of Stellar Physics on Galaxy Evolution, ed. C. Leitherer, U. F. von-Alvenskeben, & J. Huchra (San Francisco: ASP), 299
Vílchez, J. M., & Esteban, C. 1996, MNRAS, 280, 720
Weidemann, V. 1991, in Proc. 7th European Workshop on White Dwarfs, ed. G. Vauclair & E. M. Sion (Dordrecht: Kluwer), 67
Weidemann, V., & Koester, D. 1983, A&A, 121, 77
Wielen, R. 1977, A&A, 60, 263
Woosley, S. E., Langer, N., & Weaver, T. A. 1993, ApJ, 411, 823
Woosley, S. E., & Weaver, T. A. 1995, ApJS, 101, 185